ACS Sustainable Chemistry & Engineering

Research Article

pubs.acs.org/journal/ascecg

Nitrogen-Doped Hierarchical Porous Carbon Nanowhisker Ensembles on Carbon Nanofiber for High-Performance Supercapacitors

Jianan Zhang,[†] Xianglan Zhang,[†] Yunchun Zhou,[§] Shaojun Guo,*[,‡] Kaixi Wang,[†] Zhiqiang Liang,[∥] and Qun Xu*[,†]

[†]College of Materials Science and Engineering, Zhengzhou University, Zhengzhou 450052, P. R. China

[‡]Physical Chemistry and Applied Spectroscopy, Los Alamos National Laboratory, Los Alamos, New Mexico 87545, United States

[§]National Analytical Research Center of Electrochemistry and Spectroscopy, Changchun Institute of Applied Chemistry, Chinese Academy of Sciences, Changchun 130022, P. R. China

[∥]State Key Laboratory of Inorganic Synthesis and Preparation Chemistry, College of Chemistry, Jilin University, Changchun 130012, P. R. China

Supporting Information

ABSTRACT: Controlled synthesis of carbon nanomaterials with particular shape, composition, architecture, and doping is very important, yet still a great challenge, for enhancing supercapacitor performance with high energy and power densities and long lifetime. Herein, we demonstrate an interesting process combining surfactantless and templateless wet chemical and post-high-temperature carbonization strategies for obtaining a new class of nitrogen-doped hierarchical porous carbon nanowhisker ensembles supported on carbon nanofibers (NHCNs) with tunable micropores and a nitrogen-doping level for high-performance supercapacitors. Under the optimal pore size and nitrogen doping controlled by carbonization at different temperatures, the NHCNs (NHCNs-750) carbonized at 750 °C shows an optimal specific capacitance of 210.1 F g^{-1} at 5 mV s^{-1}, which is much higher than other one-dimensional carbon nanostructures (e.g., pure carbon nanofibers (2.6 F g^{-1}) and carbon nanotubes (10.6 F g^{-1}) at 5 mVs^{-1}). NHCNs-750 also showed good rate capability of 78.5% and 75.2% capacitance retention at 100 mV s^{-1} and 200 mV s^{-1}, respectively, and excellent cycling stability of 96.2% capacitance retention after 3000 cycles. Furthermore, we found that the specific capacitance of NHCNs can be further increased to 254.3 F g^{-1} by a KOH-assisted high-temperature process. The present work opens a new route to design advanced 1D hierarchical carbon nanomaterials with tunable pores and nitrogen doping for enhancing energy storage and conversion applications.

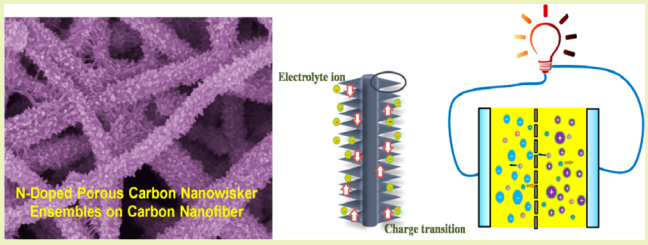

KEYWORDS: *Nanowhisker, Hierarchical structure, Carbon nanofiber, Porous structure, Supercapacitors*

INTRODUCTION

With the limited availability of fossil fuels and increasing demand for energy, tremendous attention has been paid to synthesize advanced materials for enhancing energy storage and conversion from "green" and renewable energy sources. Electrochemical capacitors (ECs) are regarded as one of the most promising future energy storage devices, especially for many portable systems and automotive applications, owing to their unique advantages including high power density, long lifespan, and good charge−discharge characteristics.[1−5] Considering the bulk materials have already reached the intrinsic limit and fail to meet the increasing demand, recently controlled synthesis of nanostrucutred materials with size, shape, composition, and architecture control has been suggested as an advanced approach to enhance the charge accumulation and ion transport in ECs.[6−9] Among them, nanostructured carbon, including carbon nanotubes (CNTs),[10−14] carbon nanofibers (CNFs),[15−18] graphene,[19−21] carbon onions,[22,23] and porous carbon nanostructures,[24−26] showed great potential in serving as vital candidates for enhancing ECs applications. Despite these great efforts, many existing carbon nanomaterials still exhibit a relatively low specific capacitance and power density due to their "dead surface" when they are used for ECs. In recent years, the construction of hierarchical nanoarchitectures with large surface areas are considered as another fundamental prerequisite to boost electrochemical and optical performances.[27−29] Prominent examples include the synthesis of flower-like Au nanoparticles (NPs) with large surface area for surface enhanced Raman spectroscopy,[30] preparation of Pt-based

Received: March 31, 2014
Revised: May 5, 2014
Published: May 12, 2014

dendritic NPs for enhancing fuel cell reactions,[31] and design of carbon-coated α-Fe_2O_3 hollow nanohorns on the CNT support for improving lithium storage capability.[32] These previous studies indicate that if 1D hierarchical carbon nanostructures with many micropores on their surface can be designed and synthesized by combing hierarchical and micropore effects further enhancement in supercapacitors may be feasible.

Molecular engineering of carbon nanomaterials, for example, nitrogen-doping, is of vital importance for enhancing electrochemical performance in the fields of fuel cells,[33,34] electrochemical capacitors,[35−38] and lithium-ion batteries[39,40] due to the fact that the lone electron pairs of nitrogen atoms provide additional negative charges into the carbon networks. Such doping effect also can significantly boost the performance of supercapacitors because the interaction between the surface nitrogen of carbon nanomaterials and electrolyte can introduce additional pseudocapacitive behavior.[41−43] These typical examples were found in recent reports in the synthesis of nitrogen-enriched CNTs originated from melamine with specific capacitance of about 167 F g^{-1}[44] and nitrogen-doped carbon materials derived from silk fibroins with specific capacitance of 52 F g^{-1}.[45] But the biggest problem for carbon nanomaterial-based ECs in the existing reports is that maximizing the nitrogen-doped surface of these materials cannot be well achieved, which leads to a relatively low actual active surface for ECs.

Herein, we demonstrate a facile route to controlled fabrication of nitrogen-doped hierarchical porous carbon nanowhisker ensembles on carbon nanofibers (NHCNs) by first controlled growth of polyaniline (PANI) nanowhisker ensembles on CNFs (PNECs) and then annealing PNECs in N_2 atmosphere at 750 °C for 2 h. The carbonization of PANI nanowhisker ensembles supported on CNFs can generate a large number of micropores and also appropriate nitrogen-containing functionalities, which are very important for enhancing both double layer capacitance and pseudocapacitance. Our electrochemical results reveal that the NHCNs (NHCNs-750) carbonized at 750 °C and show an optimal specific capacitance of 210.1 F g^{-1} at 5 mV s^{-1}, which is much higher than other one-dimensional carbon (pure carbon nanofibles (2.6 F g^{-1}) and CNTs (10.6 F g^{-1}) at 5 mVs^{-1}). NHCNs-750 also show good rate capability of 78.5% and 75.2% capacitance retention at 100 mV s^{-1} and 200 mV s^{-1}, respectively, and excellent cycling stability of 96.2% capacitance retention after 3000 cycles. Furthermore, we found that the specific capacitance of NHCNs can be further increased to 254.3 F g^{-1} by the KOH-assisted high-temperature process of NHCNs.

EXPERIMENTAL SECTION

Materials. Aniline (ANI, Tianjin Damao Chemical Reagent Factory), ammonium persulfate (APS, Sigma-Aldrich), and carbon nanofibers (CNFs, Pyrograf Products, Inc., U.S.A.) were used as received without further purification.

Preparation of NHCNs. The mixture of 3 mg of CNFs and 7 mL of 1 M $HClO_4$ solution was first sonicated until CNFs were fully dispersed. Then, 500 mL of ethanol and 10 mL of ANI monomer (10 and 25 mM) were added into the above mixture and further sonicated at 0 °C for 30 min to form a uniform solution. After that, 3 mL of 1 M $HClO_4$ solution containing APS (molar ratio of ANI/APS was 1:1) was dropwise added into the mixed solution and further stirred at 0 °C for 7 h. The dark green products were collected by centrifugation, washed with a large amount of deionized water several times, and then dried at 60 °C. The PNECs were carbonized to get NHCNs in a quartz tube at a heating rate of 5 °C min^{-1} at different temperatures of 550, 750, 950, and 1050 °C for 2 h under N_2 atmosphere. The obtained nitrogen-doped carbonaceous nanofibers were labeled as NHCNs-550, NHCNs-750, NHCNs-950, and NHCNs-1050.

KOH-Assisted Activation of NHCNs. The PNECs were precarbonized at 300 °C for 1.5 h under nitrogen atmosphere. The precarbonized materials were then mixed with KOH solid (mass ratio of KOH/carbon = 2) and annealed at 750 °C for 2 h under nitrogen atmosphere with a heating rate of 5 °C min^{-1}. The resulting dark powder was washed with 1 M HCl solution, then deionized water, followed by drying at 80 °C overnight.

Characterizations. The morphology of the samples was studied by a field-emission scanning electron microscope (FE-SEM) (JEORJSM-6700F) and a transmission electron microscope (TEM) (FEI Tecnai G2 20) with an accelerating voltage of 200 kV. The Raman measurements were performed on a Renishaw spectrometer at 532 nm on a Reishaw microscope system RM2000. X-ray diffraction (XRD) data were performed on a Y-2000 X-ray diffractometer using Cu Kα radiation (λ =1.5406 Å) at 40 kV and 40 mA. The X-ray photoelectron spectroscopy (XPS) experiments were performed with an ESCA LAB 250 spectrometer using a focused monochromatic Al Kα ($h\nu$ = 1486.6 eV) X-ray beam with a diameter of 200 μm. The nitrogen sorption experiments were carried out at 77 K on a Micromeritics Tristar2200 system with micropore analysis. The Brunauer−Emmett−Teller (BET) specific surface area was calculated using adsorption data at a relative pressure range of P/P_0 = 0.05−0.25. The pore volumes were estimated from the amounts adsorbed at a relative pressure (P/P_0) of 0.99. The micropore size distribution was calculated with the Horvath−Kawazoe (H−K) method.

Electrochemical Measurement. The electrochemical performances of the samples were characterized by cyclic voltammetry (CV), galvanostatic charge−discharge test (chronopotentionmetry, CP), cycling life measurement, and electrochemical impedance spectroscopy (EIS). The cyclic voltammetry, galvanostatic charge−discharge test, and electrochemical impedance spectroscopy were carried out on a CHI 660D electrochemical workstation (CH Instruments, Inc.). Cycling life measurement was performed using a Land battery electrochemical test CT 2001A (Jinnuo electronic Co., Ltd., Wuhan). The test electrodes were prepared by loading a slurry consisting of 80 wt % active composites, 10 wt % carbon black, and 10 wt % poly(-tetrafluoroethylene) (used as a binder, PTFE 60 wt % dispersion in H_2O, Sigma-Aldrich) on nickel foam (1 cm × 1 cm, 1.5 cm × 1.5 cm) and dried at 60 °C for 24 h. Then the electrodes were pressed at a pressure of 10 MPa for 1 min. The electrolyte was a 6.0 M KOH aqueous solution. In a three-electrode system, the smaller electrode (1 cm × 1 cm) was the test electrode. The platinum foil was the counter electrode, and the Ag/AgCl electrode was the reference electrode. The potential range of CV and CP was −1.0 to 0 V. The scan rates of cyclic voltammetry (CV) were 5, 25, 50, 100, 200, and 400 mV s^{-1}, while the galvanostatic charge−discharge tests (CP) were carried out galvanostatically at 0.5, 1.0, 2.5, 10.0, and 30.0 A g^{-1}. Electrochemical impedance spectroscopy (EIS) was measured in the frequency range of 10 mHz to 10 kHz at the open circuit voltage with an alternate current amplitude of 5 mV. In the two-electrode system, the smaller electrode (1 cm × 1 cm) was the test electrode, while the lager one (1.5 cm × 1.5 cm) was the counter electrode. The two electrodes were separated by polypropylene (PP) film. The cyclic voltammetry curves were obtained in the potential range of 0−1.0 V with scan rates of 5, 25, 50, 100, 200, and 400 mV s^{-1}. Galvanostatic charge−discharge tests were carried out galvanostatically at 0.5, 1.0, 2.5, 10.0, and 30.0 A g^{-1} over a voltage range of 0−1.0 V. Cycling life measurement was studied in the potential range of 0−1.0 V at 1.0 A g^{-1} for 3000 cycles. Electrochemical impedance spectroscopy (EIS) was measured in the frequency range of 10 mHz to 10 kHz at the open circuit voltage with an alternate current amplitude of 5 mV.

RESULTS AND DISCUSSION

The representative synthetic procedure for NHCNs is illustrated in Scheme 1. First, the commercial CNFs were

Scheme 1. Schematic Illustration for Synthetic Protocol of NHCNs

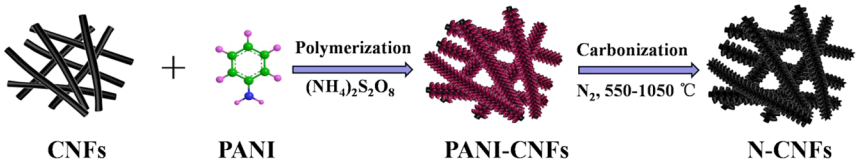

employed as the axial support to grow PANI by one-pot in situ polymerization of ANI in the presence of APS as the oxidant.[46] Figures S1 and S2 of the Supporting Information show the scanning electron microscopy (SEM) and transmission electron microscopy (TEM) images of CNFs (Figure S1) and as-prepared PNECs (Figure S2). As shown in Figure S1 of the Supporting Information, the pure CNFs with the diameter of 80−150 nm exhibit smooth surfaces, and their center presents a cup-shaped structure (inset, Figure S1b, Supporting Information). After polymerization of ANI, whisker-like PANI ensembles vertically align on the surfaces of CNFs (Figure S2, Supporting Information). The wall of the composite becomes very rough, and the average diameter increases to 220 nm. Then, the as-prepared PNECs underwent carbonization at high temperature from 550 to 1050 °C in N_2 atmosphere for 2 h at a heating rate of 5 °C min^{-1}, yielding the ordered nitrogen-doped porous carbon nanowhisker ensembles on CNFs. As shown in Figure 1a and b, all CNFs are coated with nitrogen-

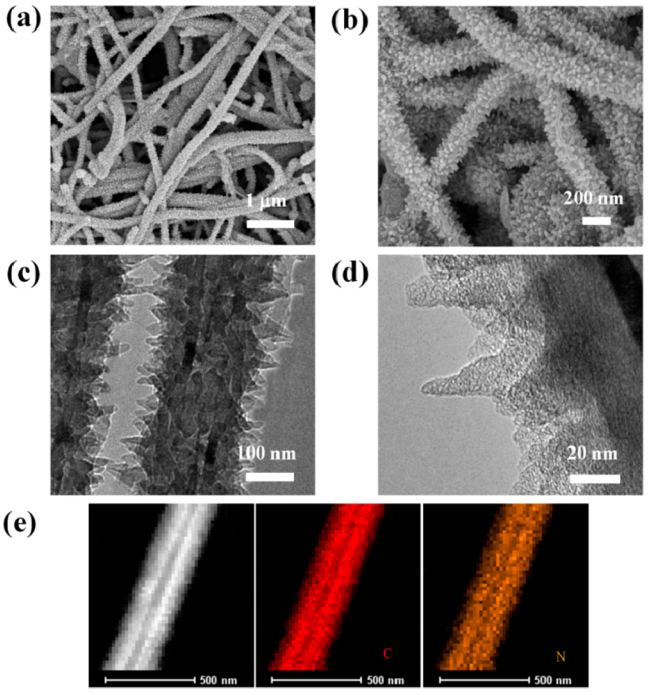

Figure 1. (a) Low-magnification SEM, (b) high-magnification SEM, and (c) TEM images of NHCNs-750. (d) HRTEM image of N-doped carbon nanowhiskers. (e) STEM mapping image of NHCNs-750.

doped carbon nanowhisper arrays. Their TEM image (Figure 1c,d) shows that the average length of the carbon nanowhiskers is ∼95 nm. A high-resolution TEM (HRTEM) image of NHCNs (Figure 1d) clearly reveals their porous structure coupled with well-defined graphitic layers, while TEM elemental mapping results (Figure 1e) show that the nitrogen and carbon in NHCNs are almost uniformly distributed on the surface of carbon nanowhisker array. Such unique structure and doping will be advantageous for enhancing the performance of supercapacitors. In addition, NHCNs with a shorter carbon nanowhisker array (average length of 55 nm, Figure S3, Supporting Information) could be facilely obtained by reducing the initial concentration of ANI from 25 to 10 mM.

To investigate the effect of carbonization temperature (T_c) on nitrogen doping and the porous structure, the as-prepared PNECs were annealed at 550, 750, 950, and 1050 °C under N_2 atmosphere to get NHCNs with different structures (designated as NHCNs-550, NHCNs-750, NHCNs-950, and NHCNs-1050). Figure 2 shows the SEM images of these

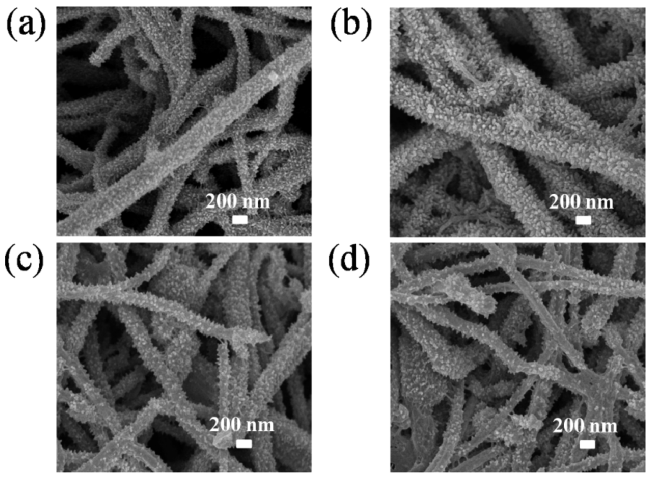

Figure 2. SEM images of NHCNs: (a) NHCNs-550, (b) NHCNs-750, (c) NHCNs-950, and (d) NHCNs-1050.

samples. With increasing the temperature from 550 to 1050 °C, the average length of the carbon nanorods decreases from 95 (Figures 2a,b) to 40 nm (Figure 2c,d) and at higher temperature some nanowhiskers even begin to decompose (Figure 2c,d).

To reveal the effect of nitrogen functionalities on capacitive performance, the type of nitrogen group introduced to NHCNs was further investigated by X-ray photoelectron spectroscopy (XPS) (Figure 3). The deconvolution of the N 1s region spectrum of NHCNs results in three type peaks correlated to different electronic states of nitrogen functional groups: pyridinic (N-6, 398.6 eV), pyrrolic/pyridine groups (N-5, 400.0 eV), and quaternary nitrogen (N-Q, 401.1 eV).[39] As shown in Figure 3a, N-5 and N-6 species are predominant for the sample with T_c below 650 °C. NHCNs-750 possesses mainly N-Q, N-6, and N-5 species (Figure 3b), attributing to the different transformation of N-5 and N-6 at different temperatures,[35,42] while no N-5 species are observed in NHCNs-950 and NHCNs-1050 (Figures 3c,d). The existence of N-Q within the graphitic structure can enhance the conductivity of carbon materials. These accessible species of N-6 and N-5 would provide chemically active sites for the

dx.doi.org/10.1021/sc500221s | ACS Sustainable Chem. Eng. 2014, 2, 1525−1533

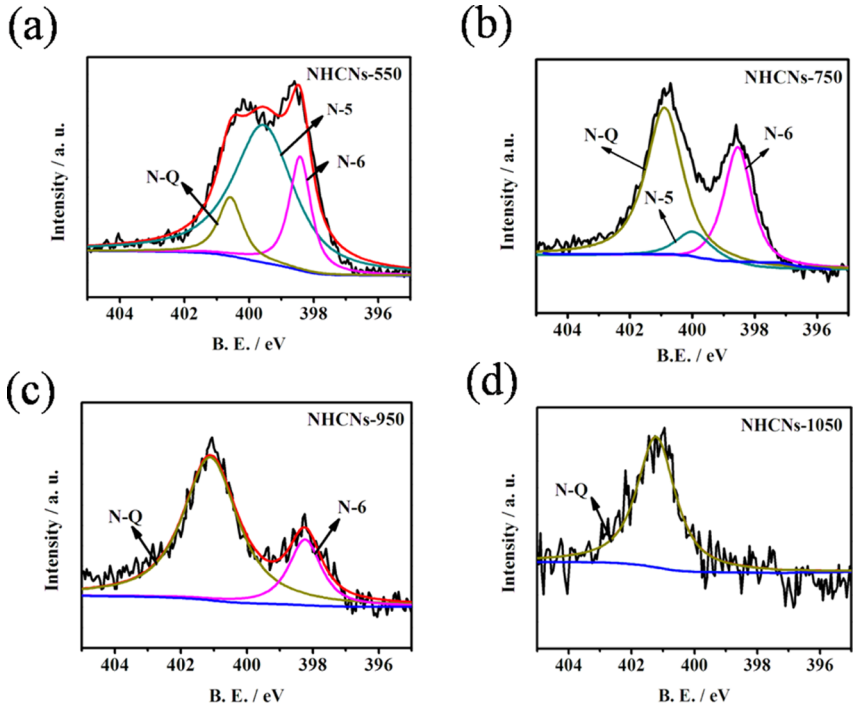

Figure 3. XPS of (a) NHCNs-550, (b) NHCNs-750, (c) NHCNs-950, and (d) NHCNs-1050.

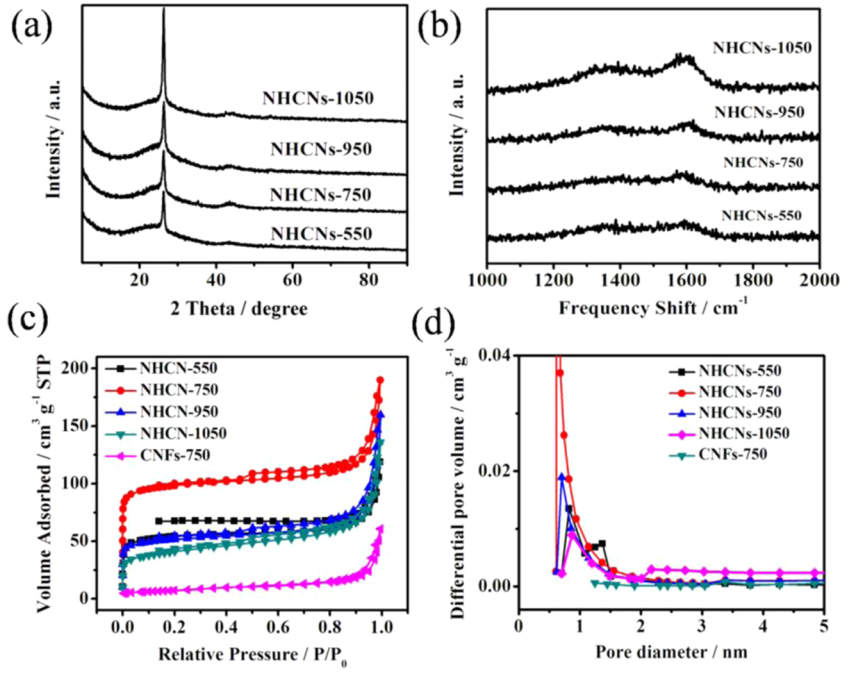

Figure 4. XRD patterns (a) and Raman spectra (b) of NHCNs-550, NHCNs-750, NHCNs-950, and NHCNs-1050. (c) N_2 adsorption−desorption isotherms and (d) pore size distribution (estimated by the adsorption isotherm) of NHCNs-550, NHCNs-750, NHCNs-950, NHCNs-1050, and CNFs-750.

pseudocapacitive reaction.[3] These results demonstrate that the carbonization temperature can affect the type of nitrogen group and thus the electrochemical performance for supercapacitors. On the basis of the XPS data from NHCNs, NHCNs-750 is expected to have a higher electrochemical performance than others.

Figure 4a shows the wide-angle powder X-ray diffraction (XRD) pattern of NHCNs treated with different temperatures. The materials exhibit a sharp peak at the 2θ = 26.5° and a broad peak at 43.5°, which correspond to (002) and (101) reflection of pure graphitic lattice (JCPDS, Card No. 75-1621), respectively. Particularly, for NHCNs-750, NHCNs-950, and NHCNs-1050, with the increase in the carbonization temperature, the intensity of the peak at 26.5° gradually increases, whereas their full width at half-maximum decreases. The intensity of the other peak at 43.5° increases a little with T_c. These results suggest that the degree of graphitization becomes higher with the increase in T_c. This observation was also proven

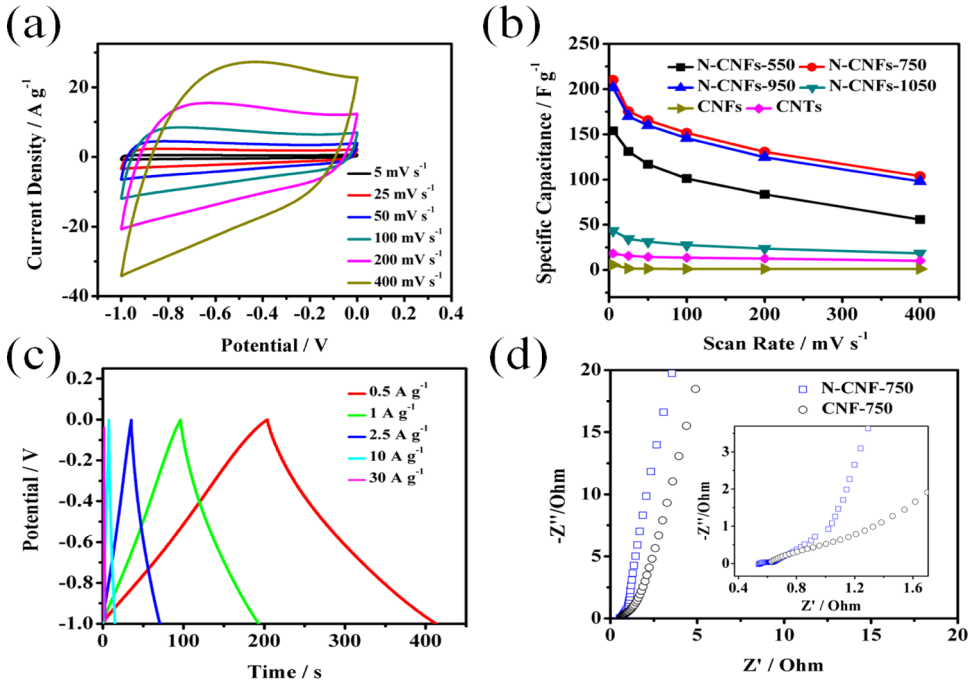

Figure 5. Electrochemical performances measured in a three-electrode system. (a) Cyclic voltammograms of the NHCN-750 electrode at different scan rates. (b) Specific capacitances of NHCN-550, NHCN-750, NHCN-950, NHCN-1050, and CNFs electrodes at different scan rates. (c) Galvanostatic charge−discharge curves of NHCN-750 at different current densities. (d) Electrochemical impedance spectra measured in the frequency range of 10 mHz to 10 kHz at the open circuit voltage with an alternate current amplitude of 5 mV.

by Raman spectra of different annealed samples (Figure 4b). As is known, the broad peaks with low intensity for D-band (1345 cm^{-1}) and high intensity for G-band (1580 cm^{-1}) indicate the as-prepared NHCNs contain both disordered and graphitic structures, respectively.[47] The intensity ratio of I_G/I_D increases with the carbonization temperature, indicating that the graphitic degree of the NHCNs increases in the order of NHCNs-1050 > NHCNs-950 > NHCNs-750 > NHCNs-550, which is well in agreement with XRD data, reflecting that better crystallization occurs at higher T_c.

We further used the nitrogen sorption measurement to analyze the porous structures of the NHCNs (Figure 4c,d). Figure 4c shows the N_2 adsorption−desorption isotherms of NHCNs-550, NHCNs-750, NHCNs-950, NHCNs-1050, and CNFs-750. A distinct hysteresis loop extending from P/P_0 = 0.4 to 1.0 with steep uptakes below P/P_0 = 0.01 were observed in the type IV (IUPAC classification) isotherm of all NHCNs, indicating the coexistence of micropores in these samples, while CNFs-750 only shows a small hysteresis loop at the range of P/P_0 = 0.9−1.0. As summarized in Table S1 of the Supporting Information, the Brunauer−Emmett−Teller (BET) surface areas of NHCNs (surface areas of NHCNs-550, NHCNs-750, NHCNs-950, and NHCNs-1050 are 184.67, 331.16, 174.15, and 141.53 m g^{-1}, respectively) are much higher than that of CNFs-750 (25.05 m g^{-1}). This indicates that the remarkable enhancement of surface area for NHCNs relative to original CNFs comes from the contribution of porous carbon nanowiskers. The decrease in surface area with the increase in T_c is mainly attributed to the decomposition and shrinkage of carbon nanowiskers, well consistent with SEM results (Figure 2). Figure 4d gives the pore size distribution (PSD) curves of all samples. The PSDs of NHCNs are mainly in the microporous region (0−2.0 nm). Typically, NHCNs-750 shows a sharp peak at 0.74 nm, while NHCNs-550, NHCNs-950, and NHCNs-1050 show relatively less microporous structures. The dominant of microporous structure for NHCNs-750 may be helpful for its performance for ECs.

In order to verify the effectiveness of NHCNs as new electrode materials for supercapacitors, cyclic voltammetry (CV), galvanostatic charge−discharge, and electrochemical impedance spectroscopy (EIS) were measured in a 6 M KOH aqueous electrolyte with a three-electrode configuration (Figure 5 and Figure S4, Supporting Information). The CV curves of all NHCNs are depicted in Figure S4 of the Supporting Information. All samples present capacitive behavior with roughly rectangular-like shapes and reversible bumps in CV curves, being attributed to the combination of electric double-layer capacitance (EDLC) and pseudocapacitive reaction.[41−43] Particularly, the rectangular shape of all NHCNs can be kept even at a potential scan rate of 400 mV s^{-1} (Figure 5a), indicating a good rate capability for NHCNs. The specific capacitance can be calculated from CV curves according to the following equation.[48,49]

$$C_s = \frac{1}{m\varphi(V_2 - V_1)} \int_{V_2}^{V_1} I\,dV \qquad (1)$$

where C_s (F g^{-1}) is the specific capacitance, φ (V s^{-1}) is the scanning rate, V (V) is the scanning voltage, and m (g) is the mass of active materials within the electrode. The correlation of C_s for 1D-based carbon nanostrucutres versus the scan rate is shown in Figure 5b. Obviously, NHCNs carbonized at 750 °C display a substantially higher specific capacitance than other NHCNs as well as the commercial pure CNFs and multi-walled CNTs. For example, at a given scan rate of 5 mV s^{-1}, the C_s of NHCNs-550, NHCNs-750, NHCNs-950, NHCNs-1050, CNFs, and multi-walled CNTs are 153.9, 210.1, 201.5, 43.4, 5.9, and 18.2 F g^{-1}, respectively. It should be noted that NHCNs-950 and NHCNs-1050 display relative lower C_s values

dx.doi.org/10.1021/sc500221s | ACS Sustainable Chem. Eng. 2014, 2, 1525−1533

Table 1. Physicochemical Properties of All Nitrogen-Doped Carbon Nanowhiskers on CNFs and Pure CNFs

	NHCNs-550	NHCNs-750	NHCNs-950	NHCNs-1050	CNFs-750
BET surface area ($m^2\ g^{-1}$)	184.67	331.16	174.15	141.53	25.05
t-method external surface area ($m^2\ g^{-1}$)	53.83	65.26	48.98	71.72	22.44
total pore volume ($cm^3\ g^{-1}$)	0.13	0.22	0.16	0.14	0.053
average pore diameter (nm)	2.89	2.68	3.60	3.97	8.40

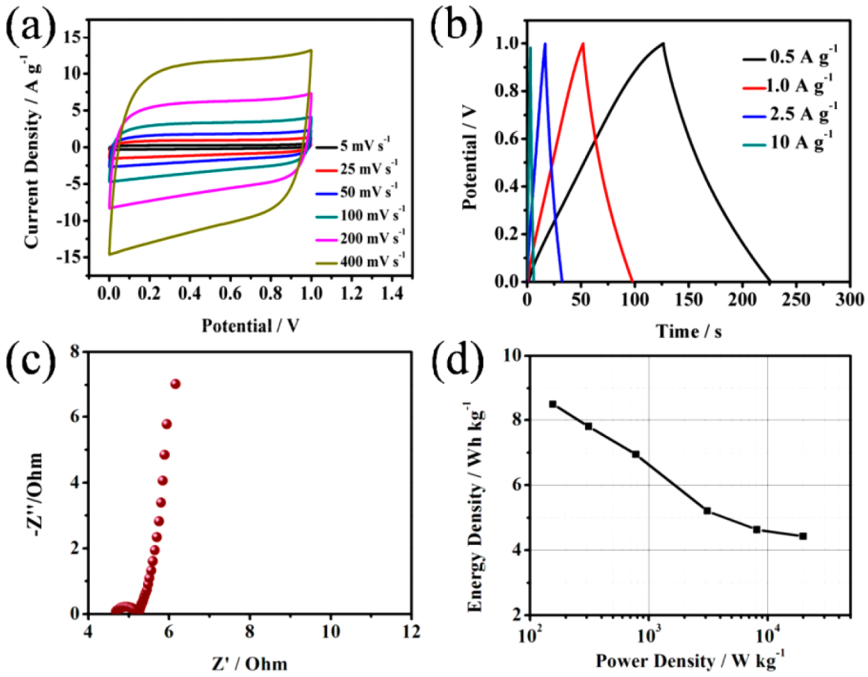

Figure 6. Electrochemical performances of the NHCNs-750//NHCNs-750-based supercapacitor measured in a two-electrode system. (a) CV curves at different scan rates. (b) Galvanostatic charge−discharge curves at different current densities. (c) EIS curve measured in the frequency range from 10 mHz to 10 kHz at the open circuit voltage with an alternate current amplitude of 5 mV. (d) Ragone plot of the NHCN-750//N-CNF-750 device performed in a 6.0 MKOH aqueous solution.

even if they exhibit higher graphitic structures than NHCNs-750. This is because the higher temperature treatment on NHCNs will make them lose their surface area (Table 1) and also reduce their nitrogen-doping amount (dopings of N-CNFs-550, N-CNFs-750, N-CNFs-950, and N-CNFs-1050 are 13.6, 10.9, 6.2, and 2.4%, respectively, revealed by Figure 3). Therefore, the enhancement of NHCNs-750 for the supercapacitor can be attributed to the synergistic effects of the optimal large accessible surface area (improving the transport of electrolyte ions), an optimal nitrogen-doping level (changing the electron donor/acceptor characteristics of carbon), and their high conductivity. Furthermore, NHCNs-750 also exhibit good rate capability of 78.5% and 75.2% capacitance retention at 100 mV s^{-1} and 200 mV s^{-1}, respectively. Galvanostatic charge−discharge tests performed at various current densities at the potential range from −1.0 to 0 V are shown in Figure 5c. We found that the typical charge−discharge curves of NHCN-750 at different current densities are nearly linear and symmetric with a gradual slop change, exhibiting an ideal capacitor behavior.

A symmetrical two-electrode configuration was utilized to further determine the electrochemical performance of the NHCNs-750 in a 6 M KOH aqueous solution (Figure 6). As shown in Figure 6a, the CVs of the NHCNs-750//NHCNs-750 device at different scan rates present a "rectangular shape" even at a high potential scan rate of 400 mV s^{-1}, further indicating its good rate capability. The power density and energy density are powerful information regarding the electrochemical performance of electrode materials, and they are estimated using the galvanostatic charge−discharge and EIS data (Figure 6b,c) in eqs 2−4).[35,50−53]

$$C_s = \frac{i \times \Delta t}{M \times \Delta V} \tag{2}$$

$$E = \frac{1}{2} C_m (\Delta V) \tag{3}$$

$$P_{av} = \frac{E}{\Delta t} \tag{4}$$

where C_s (F g^{-1}) is the measured device capacitance, i (A) represents the discharge current, ΔV (V) is the voltage change (excluding the iR drop) within the discharge time, M (g) refers to the total mass of the active two electrodes, and E (J g^{-1}) and P_{av} (W g^{-1}) represents the energy density and power density, respectively. Figure 6d gives the Ragone plot for the NHCNs-750//NHCNs-750 device in a 6.0 M aqueous KOH electrolyte. The specific energy density is as high as 8.5 Wh kg^{-1} at a current density of 0.5 A g^{-1}. Moreover, the specific energy densities are kept at 4.6 and 4.5 Wh kg^{-1} with high specific power densities of 8.1 and 20.0 kW kg^{-1} at high current densities of 15 and 30 A g^{-1}, respectively, which is much better than those of active carbon (3−4 kW kg^{-1})[54] and nitrogen-doped carbon fiber.[35] The stability of the NHCNs-750//

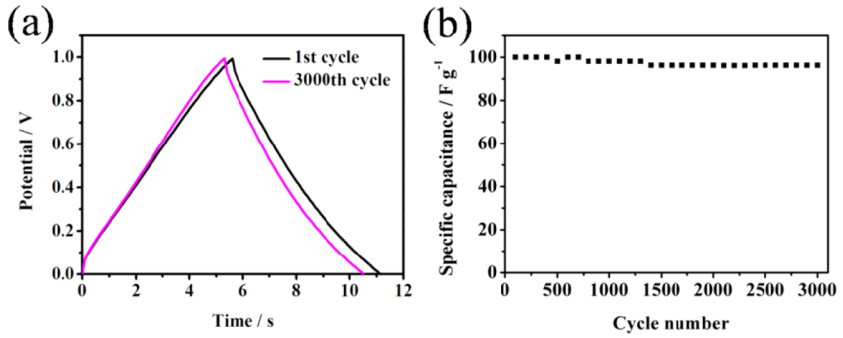

Figure 7. (a) Galvanostatic charge–discharge curves of the NHCN-750//N-CNF-750 device before and after 3000 cycles at a 5 A g^{-1}. (b) Capacitance retention vs cycle number measured at 5 A g^{-1}.

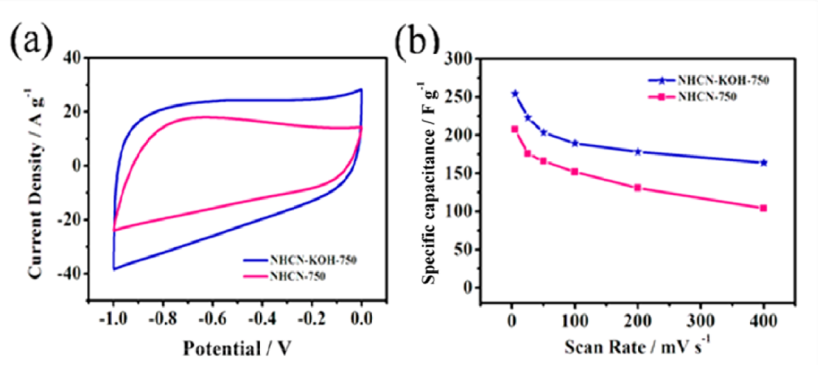

Figure 8. (a) CV curves of NHCN-KOH-750 and NHCN-750 at 200 mV s^{-1}. (b) Correlation of specific capacitances for NHCN-KOH-750 and NHCN-750.

NHCNs-750 device was evaluated by galvanostatic charge–discharge tests at a galvanostatic charge–discharge current density of 5 A g^{-1}. As shown in Figure 7, the capacitance retention of the NHCNs-750//NHCNs-750 device still remains 96.2% after a 3000 cycle, indicating its excellent cycling stability.

In order to improve the supercapacitor performance of NHCNs-750, we further activated it through a KOH-assisted high-temperature annealing process in nitrogen atmosphere, adopted from a recent report.[55] The obtained material is noted as NHCNs-KOH-750. Figure S5 of the Supporting Information shows the TEM image of NHCNs-KOH-750. After KOH active treatment, the carbon nanowhisker ensembles transfer to carbon nanosheets with microporous and mesoporous structures, implying a remarkable improvement in surface area. The CVs (Figure 8a) and corresponding C_s (Figure 8b) of NHCNs-750 and NHCNs-KOH-750 are shown in Figure 8. Compared with NHNCs-750, KOH-activated NHCNs-750 shows enhanced higher capacitance (254.3 F g^{-1}), indicating that through rational tuning on the structure and pores (surfaces area is 1606 m^2 g) of NHNCs-750, we can further tune the supercapacitor performance.

CONCLUSIONS

We successfully demonstrated a multi-step process for the preparation of a new class of hierarchical 1D nitrogen-doped porous carbon nanowhiskers supported on CNFs through first the polymerization of aniline on the CNFs and then annealing the nanocomposite at high temperature in the N_2 atmosphere. The pore size and nitrogen-doping level on carbon nanowhispers can be easily tuned by simply changing the calcination temperature from 550 to 1050 °C. Such multiple scale tunings on hierarchical nanostructures, nitrogen doping, and porosity endow the NHCNs with good capacitive performance for supercapacitors. Electrochemical studies demonstrate that the NHCNs and KOH-activated NHCNs carbonized at 750 °C show the optimal specific capacitances of 210.1 and 254.3 F g^{-1}, respectively, much higher than those of other one-dimensional carbon nanostructures such as pure CNFs and CNTs, and a long cycle life. The results demonstrate that NHCNs are a very promising candidate for future high performance supercapacitors.

ASSOCIATED CONTENT

Supporting Information

SEM images of CNFs, CNFs/PANI, and NHCNs-750; TEM images of CNFs, CNFs/PANI, and NHCNs-KOH-750; CV curves of samples at different scan rates. This material is available free of charge via the Internet at http://pubs.acs.org.

AUTHOR INFORMATION

Corresponding Authors

*E-mail: shaojun.guo.nano@gmail.com (S.G.).
*E-mail: qunxu@zzu.edu.cn (Q.X.).

Author Contributions

J. Zhang designed the experimental scheme, guided the work, and participated in the writing of the article. X. Zhang completed the experimental section and also contributed to the writing. Y. Zhou helped complete the test of TEM and helped solve some difficulties. S. Guo carried out the tests of XRD and Raman. K. Wang assisted us in the schematic illustration and helped with the experiment. Z. Liang carried out the test of XPS. Q. Xu reviewed the manuscript and helped with the work.

Notes

The authors declare no competing financial interest.

■ ACKNOWLEDGMENTS

This work was financially supported by the National Natural Science Foundation of China (21101141 and 51202223), Program for New Century Excellent Talents in Universities (NCET), J. Robert Oppenheimer Distinguished Fellowship, and Open Project Foundation of State Key Laboratory of Inorganic Synthesis and Preparation Chemistry of Jilin University (2012-13).

■ REFERENCES

(1) Hochbaum, A. I.; Yang, P. Semiconductor nanowires for energy conversion. *Chem. Rev.* **2009**, *110*, 527−546.
(2) Miller, J. R.; Simon, P. Electrochemical Capacitors for energy management. *Science* **2008**, *321*, 651−652.
(3) Su, F. B.; Poh, C. K.; Chen, J. S.; Xu, G. W.; Wang, D.; Li, Q.; Lin, J. Y.; Lou, X. W. Nitrogen-containing micro-porous carbon nanospheres with improved capacitive properties. *Energy Environ. Sci.* **2011**, *4*, 717−724.
(4) Jiang, J.; Li, Y.; Liu, J.; Huang, X.; Yuan, C.; Lou, X. W. Recent advances in metal oxide-based electrode architecture design for electrochemical energy storage. *Adv. Mater.* **2012**, *24*, 5166−80.
(5) Zhai, Y.; Dou, Y.; Zhao, D.; Fulvio, P. F.; Mayes, R. T.; Dai, S. Carbon materials for chemical capacitive energy storage. *Adv. Mater.* **2011**, *23*, 4828−4850.
(6) Vijayakumar, S.; Nagamuthu, S.; Muralidharan, G. Porous NiO/C nanocomposites as electrode material forelectrochemical supercapacitors. *ACS Sustainable Chem. Eng.* **2013**, *1*, 1110−1118.
(7) Liang, C.; Li, Z.; Dai, S. Mesoporous carbon materials: Synthesis and modification. *Angew. Chem., Int. Ed.* **2008**, *47*, 3696−3717.
(8) Liu, C.; Li, F.; Ma, L.; Cheng, H. Advanced materials for energy storage. *Adv. Mater.* **2010**, *22*, E28−E62.
(9) Xiao, L.; Cao, Y.; Xiao, J.; Schwenzer, B.; Engelhard, M. H.; Saraf, L. V.; Nie, Z.; Exarhos, G. J.; Liu, J. A soft approach to encapsulate sulfur: polyaniline nanotubes for lithium-sulfur batteries with long cycle life. *Adv. Mater.* **2012**, *24*, 1176−1181.
(10) Sevilla, M.; Yu, L.; Zhao, L.; Ania, C. O.; Titiricic, M.-M. Research article surface modification of CNTs with N-doped carbon: An effective way of enhancing their performance in supercapacitors. *ACS Sustainable Chem. Eng.* **2014**, *2*, 1049−1055.
(11) Izadi-Najafabadi, A.; Yamada, T.; Futaba, D. N.; Yudasaka, M.; Takagi, H.; Hatori, H.; Iijima, S.; Hata, K. High-power supercapacitor electrodes from single-walled carbon nanohorn/nanotube composite. *ACS Nano* **2011**, *5*, 811−819.
(12) Hahm, M. G.; Leela Mohana Reddy, A.; Cole, D. P.; Rivera, M.; Vento, J. A.; Nam, J.; Jung, H. Y.; Kim, Y. L.; Narayanan, N. T.; Hashim, D. P.; Galande, C.; Jung, Y. J.; Bundy, M.; Karna, S.; Ajayan, P. M.; Vajtai, R. Carbon nanotube−nanocup hybrid structures for high power supercapacitor applications. *Nano Lett.* **2012**, *12*, 5616−5621.
(13) Jiang, H.; Li, C. Z.; Sun, T.; Ma, J. A green and high energy density asymmetric supercapacitor based on ultrathin MnO_2 nanostructures and functional mesoporous carbon nanotube electrodes. *Nanoscale* **2012**, *4*, 807−812.
(14) Li, P. X.; Kong, C. Y.; Shang, Y. Y.; Shi, E. Z.; Yu, Y. T.; Qian, W. Z.; Wei, F.; Wei, J. Q.; Wang, K. L.; Zhu, H. W.; Cao, A. Y.; Wu, D. H. Highly deformation-tolerant carbon nanotube sponges as supercapacitor electrodes. *Nanoscale* **2013**, *5*, 8472−8479.
(15) Cao, Y.; Zhu, M.; Li, P.; Zhang, R.; Li, X.; Gong, Q.; Wang, K.; Zhong, M.; Wu, D.; Lin, F.; Zhu, H. Boosting supercapacitor performance of carbon fibres using electrochemically reduced graphene oxide additives. *Phys. Chem. Chem. Phys.* **2013**, *15*, 19550−19556.
(16) Qian, H.; Kucernak, A. R.; Greenhalgh, E. S.; Bismarck, A.; Shaffer, M. S. P. Multifunctional structural supercapacitor composites based on carbon aerogel modified high performance carbon fiber fabric. *ACS Appl. Mater. Interfaces* **2013**, *5*, 6113−6122.
(17) Ren, J.; Li, L.; Chen, C.; Chen, X.; Cai, Z.; Qiu, L.; Wang, Y.; Zhu, X.; Peng, H. Twisting carbon nanotube fibers for both wire-shaped micro-supercapacitor and micro-battery. *Adv. Mater.* **2013**, *25*, 1155−1159.
(18) Le, V. T.; Kim, H.; Ghosh, A.; Kim, J.; Chang, J.; Quoc, A. V.; Pham, D. T.; Lee, J.-H.; Kim, S.-W.; Lee, Y. H. Coaxial fiber supercapacitor using all-carbon material electrodes. *ACS Nano* **2013**, *7*, 5940−5947.
(19) Wei, A.; Weiwei, Z.; Zhuzhu, D.; Yaping, D.; Hua, Z.; Xingtao, J.; Linghai, X.; Mingdong, Y.; Ting, Y.; Wei, H. Benzoxazole and benzimidazole heterocycle-grafted graphene for high-performance supercapacitor electrodes. *J. Mater. Chem.* **2012**, *22*, 23439−23446.
(20) Zhang, L.; Shi, G. Preparation of highly conductive graphene hydrogels for fabricating supercapacitors with high rate capability. *J. Phys. Chem. C* **2011**, *115* (34), 17206−17212.
(21) Wu, Z.; Ren, W.; Gao, L.; Zhao, J.; Chen, Z.; Liu, B.; Tang, D.; Yu, B.; Jiang, C.; Cheng, H. Synthesis of graphene sheets with high electrical conductivity and good thermal stability by hydrogen arc discharge exfoliation. *ACS Nano* **2009**, *3*, 411−417.
(22) Portet, C.; Yushin, G.; Gogotsi, Y. Electrochemical performance of carbon onions, nanodiamonds, carbon black and multiwalled nanotubes in electrical double layer capacitors. *Carbon* **2007**, *45*, 2511−2518.
(23) Pech, D.; Brunet, M.; Durou, H.; Huang, P.; Mochalin, V.; Gogotsi, Y.; Taberna, P.-L.; Simon, P. Ultrahigh-power micrometre-sized supercapacitors based on onion-like carbon. *Nat. Nanotechnol.* **2010**, *5*, 651−654.
(24) Candelaria, S. L.; Garcia, B. B.; Liu, D.; Cao, G. Nitrogen modification of highly porous carbon for improved supercapacitor performance. *J. Mater. Chem.* **2012**, *22*, 9884−9889.
(25) Estevez, L.; Dua, R.; Bhandari, N.; Ramanujapuram, A.; Wang, P.; Giannelis, E. P. A facile approach for the synthesis of monolithic hierarchical porous carbons−high performance materials for amine based CO_2 capture and supercapacitor electrode. *Energy Environ. Sci.* **2013**, *6*, 1785−1790.
(26) Liu, X.; Zhou, L.; Zhao, Y.; Bian, L.; Feng, X.; Pu, Q. Hollow, spherical nitrogen-rich porous carbon shells obtained from a porous organic framework for the supercapacitor. *ACS Appl. Mater. Interfaces* **2013**, *5*, 10280−10287.
(27) Jiang, J.; Li, Y.; Liu, J.; Huang, X. Building one-dimensional oxide nanostructure arrays on conductive metal substrates for lithium-ion battery anodes. *Nanoscale* **2011**, *3*, 45−58.
(28) Chen, Q.; Li, H.; Cai, C.; Yang, S.; Huang, K.; Weiab, X.; Zhong, J. *In situ* shape and phase transformation synthesis of Co_3S_4 nanosheet arrays for high-performance electrochemical supercapacitors. *RSC Adv.* **2013**, *3*, 22922−22926.
(29) Yang, L.; Cheng, S.; Ding, Y.; Zhu, X. B.; Wang, Z. L.; Liu, M. L. Hierarchical network architectures of carbon fiber paper supported cobalt oxide nanonet for high-capacity pseudocapacitors. *Nano Lett.* **2012**, *12*, 321−325.
(30) Guo, S.; Wang, L.; Wang, E. Templateless, surfactantless, simple electrochemical route to rapid synthesis of diameter-controlled 3D flowerlike gold microstructure with "clean" surface. *Chem. Commun.* **2007**, 3163−3165.
(31) Wang, L.; Yamauchi, Y. Block copolymer mediated synthesis of dendritic platinum nanoparticles. *J. Am. Chem. Soc.* **2009**, *131*, 9152−9153.
(32) Wang, Z.; Luan, D.; Madhavi, S.; Hu, Y.; Lou, X. W. D. Assembling carbon-coated α-Fe_2O_3 hollow nanohorns on the CNT backbone for superior lithium storage capability. *Energy Environ. Sci.* **2012**, *5*, 5252−5256.
(33) Qu, L.; Liu, Y.; Baek, J.-B.; Dai, L. Nitrogen-doped graphene as efficient metal-free electrocatalyst for oxygen reduction in fuel cells. *ACS Nano* **2010**, *4*, 1321−1326.
(34) Chen, Z.; Higgins, D.; Tao, H. S.; Hsu, R.-S.; Chen, Z. W. Highly active nitrogen-doped carbon nanotubes for oxygen reduction reaction in fuel cell applications. *J. Phys. Chem. C* **2009**, *113*, 21008−21013.

(35) Chen, L.; Zhang, X.; Liang, H.; Kong, M.; Guan, Q.; Chen, P.; Wu, Z.; Yu, S. Synthesis of nitrogen-doped porous carbon nanofibers as an efficient electrode material for supercapacitors. *ACS Nano* **2012**, *6*, 7092−7102.
(36) Tsubota, T.; Takenaka, K.; Murakami, N.; Ohno, T. Performance of nitrogen- and sulfur-containing carbon material derived from thiourea and formaldehyde as electrochemical capacitor. *J. Power Sources* **2011**, *196*, 10455−10460.
(37) Wooyoung, K.; Mi Yeong, K.; Ji Bong, J.; Nam Dong, K.; In Kyu, S.; Pil, K.; Jung Rag, Y.; Jongheop, Y. Preparation of ordered mesoporous carbon nanopipes with controlled nitrogen species for application in electrical double-layer capacitors. *J. Power Sources* **2010**, *195*, 2125−21259.
(38) Kim, W.; Joo, J. B.; Kim, N.; Oh, S.; Kim, P.; Yi, J. Preparation of nitrogen-doped mesoporous carbon nanopipes for the electrochemical double layer capacitor. *Carbon* **2009**, *47*, 1407−1411.
(39) Reddy, A. L. M.; Srivastava, A.; Gowda, S. R.; Gullapalli, H.; Dubey, M.; Ajayan, P. M. Synthesis of nitrogen-doped graphene films for lithium battery application. *ACS Nano* **2010**, *4*, 6337−6342.
(40) Qie, L.; Chen, W. M.; Wang, Z. H.; Shao, Q. G.; Li, X.; Yuan, L. X.; Hu, X. L.; Zhang, W. X.; Huang, Y. H. Nitrogen-doped porous carbon nanofiber webs as anodes for lithium ion batteries with a superhigh capacity and rate capability. *Adv. Mater.* **2012**, *24*, 2047−2050.
(41) Seredych, M.; Hulicova Jurcakova, D.; Lu, G. Q.; Bandosz, T. J. Surface functional groups of carbons and the effects of their chemical character, density and accessibility to ions on electrochemical performance. *Carbon* **2008**, *46*, 1475−1488.
(42) Hulicova Jurcakova, D.; Seredych, M.; Lu, G. Q.; Bandosz, T. J. Combined effect of nitrogen- and oxygen-containing functional groups of microporous activated carbon on its electrochemical performance in supercapacitors. *Adv. Funct. Mater.* **2009**, *19*, 438−447.
(43) Tan, Y.; Xu, C.; Chen, G.; Liu, Z.; Ma, M.; Xie, Q.; Zheng, N.; Yao, S. Synthesis of ultrathin nitrogen-doped graphitic carbon nanocages as advanced electrode materials for supercapacitor. *ACS Appl. Mater. Interfaces* **2013**, *5*, 2241−2248.
(44) Jurewicz, K.; Babeł, K.; Ziółkowski, A.; Wachowska, H. Capacitance behaviour of the ammoxidised coal. *J. Phys. Chem. Solids* **2004**, *65*, 269−273.
(45) Kim, Y. J.; Abe, Y.; Yanagiura, T.; Park, K. C.; Shimizu, M.; Iwazaki, T.; Nakagawa, S.; Endo, M.; Dresselhaus, M. S. Easy preparation of nitrogen-enriched carbon materials from peptides of silk fibroins and their use to produce a high volumetric energy density in supercapacitors. *Carbon* **2007**, *45*, 2116−2125.
(46) Wei, J.; Zhang, J.; Liu, Y.; Xu, G.; Chen, Z.; Xu, Q. Controlled growth of whisker-like polyaniline on carbon nanofibers and their long cycle life for supercapacitors. *RSC Adv.* **2013**, *3*, 3957−3962.
(47) Wang, Y.; Su, F.; Wood, C. D.; Lee, J. Y.; Zhao, X. S. Preparation and characterization of carbon nanospheres as anode materials in lithium-ion secondary batteries. *Ind. Eng. Chem. Res.* **2008**, *47*, 2294−2300.
(48) Stoller, M. D.; Ruoff, R. S. Best practice methods for determining an electrodematerial's performance for ultracapacitors. *Energy Environ. Sci.* **2010**, *3*, 1294−1301.
(49) Zhang, L. L.; Zhao, X. S. Carbon-based materials as supercapacitor electrodes. *Chem. Soc. Rev.* **2009**, *38*, 2520−2531.
(50) Hu, H.; Zhao, Z.; Zhou, Q.; Gogotsi, Y.; Qiu, J. The role of microwave absorption on formation of graphene from graphite oxide. *Carbon* **2012**, *50*, 3267−3273.
(51) Lin, R.; Taberna, P. L.; Fantini, S.; Presser, V.; Pérez, C. R.; Malbosc, F.; Rupesinghe, N. L.; Teo, K. B.; Gogotsi, Y.; Simon, P. Capacitive energy storage from −50 to 100 °C using an ionic liquid electrolyte. *J. Phys. Chem. Lett.* **2011**, *2*, 2396−2401.
(52) Yan, J.; Wei, T.; Qiao, W.; Fan, Z.; Zhang, L.; Li, T.; Zhao, Q. A high-performance carbon derived from polyaniline for supercapacitors. *Electrochem. Commun.* **2010**, *12*, 1279−1282.
(53) Jeong, H. M.; Lee, J. W.; Shin, W. H.; Choi, Y. J.; Shin, H. J.; Kang, J. K.; Choi, J. W. Nitrogen-doped graphene for high-performance ultracapacitors and the importance of nitrogen-doped sites at basal planes. *Nano Lett.* **2011**, *11*, 2472−2477.
(54) Fan, Z.; Yan, J.; Wei, T.; Zhi, L.; Ning, G.; Li, T.; Wei, F. Asymmetric supercapacitors based on graphene/MnO_2 and activated carbon nanofiber electrodes with high power and energy density. *Adv. Funct. Mater.* **2011**, *21*, 2366−2375.
(55) Qian, W.; Sun, F.; Xu, Y.; Qiu, L.; Liu, C.; Wang, S.; Yan, F. Human hair-derived carbon flakes for electrochemical supercapacitors. *Energy Environ. Sci.* **2014**, *7*, 379−386.